Two-dimensional model problem to explain counter-rotating vortex pair formation in a transverse jet

Suman Muppidi and Krishnan Mahesh
Aerospace Engineering & Mechanics, University of Minnesota, Minneapolis, Minnesota 55455

(Received 20 January 2006; accepted 26 June 2006; published online 17 August 2006)

A two-dimensional model problem is used to study the evolution of the cross section of a transverse jet and the counter-rotating vortex pair (CVP). The solution to the model problem shows deformation of the jet similar to that observed in a transverse jet, and also yields a CVP. These phenomena are explained in terms of the acceleration the jet experiences in the direction of the cross-flow, and the pressure field around the jet. The initial stages of the jet's evolution are at constant acceleration while the later stages are at constant velocity. The effects of Reynolds number and velocity ratio on the evolution of the jet are used to explain the dependence of CVP formation on velocity ratio, as observed by Smith and Mungal [J. Fluid Mech. **357**, 83 (1998)]. © *2006 American Institute of Physics*. [DOI: 10.1063/1.2236304]

I. INTRODUCTION

A circular jet issuing into a cross-flow bends in the direction of the cross-flow. As the jet bends, the jet cross section deforms and a pair of counter-rotating vortices (CVPs) are formed. The CVP is a "signature" feature of this flow and has been the subject of much investigation. Detailed measurements of velocity and vorticity fields in the cross section of the CVP have been performed,[1,2] and the CVP has been observed to persist far downstream.[3–5] Smith and Mungal[6] report that the CVP formation appears slower at $r=20$ than at $r=10$ (as a function of the nondimensional distance variable x/rd). The CVP is credited with the enhanced mixing observed in transverse jets as compared to free jets.

Stages in the evolution of a transverse jet are shown in Fig. 1, using contours of out-of-plane velocity on planes normal to the trajectory. The direction of the cross-flow fluid is from the left to the right. Note the increase in size of the jet cross section with distance from the jet exit. Close to the jet exit, fluid with the highest velocity is seen toward the center of the jet cross section. Away from the jet exit, the high velocity contours are observed toward the edges of the jet, while fluid toward the center appears to have a relatively lower velocity. The figures also show a few representative in-plane streamlines, which reveal a CVP trailing the jet cross section. The CVP increases in size along the jet length.

Different mechanisms leading to the CVP have been suggested. Broadwell and Breidenthal[7] model the jet as a point source of momentum. This results in a "lift force of vanishing drag" and generates the CVP, similar to the wing tip vortices observed in a flow past a wing. It has also been suggested (e.g., Ref. 8) that the CVP is formed by the shear layer emanating from the pipe. Coelho and Hunt[9] suggest that the CVP is initiated within the pipe. Kelso *et al.*[5] conclude from their experiments that CVP roll-up is related to the separation inside the pipe and that the "folding" of the jet shear layer contributes to the circulation of the CVP. Cortelezzi and Karagozian[10] simulate the flow field using vortex elements, in a domain that does not include the pipe, and agree with the mechanism proposed by Kelso *et al.*[5]

Karagozian[11] models the jet as two curved, semi-infinite, vortex lines originating near the jet exit. Equations governing vortex spacing and jet velocity are numerically solved, and theoretical prediction of parameters such as vortex trajectory agree reasonably with experimental results. It is concluded that the effect of jet velocity on the vortex strength becomes apparent only in the far field, once the jet has been deflected by the cross-flow. By relating the circulation of the CVP to the impulse (of the jet) and using similarity arguments, Broadwell and Breidenthal[7] obtain scaling laws for jet trajectory in the far field. Both of these models assume that the CVP is present along the length of the jet, and that the flow in the far-field is locally two dimensional.

The objective of this paper is to suggest that the formation of the CVP may be explained using a two-dimensional model problem. The solution to this problem shows that CVP formation and the jet cross-section deformation can be understood as a consequence of the cross-flow fluid accelerating the jet in the streamwise direction. It also shows that the pipe is not necessary to generate the CVP. The model problem is solved using direct numerical simulations. The paper is organized as follows. The model problem is described in Sec. II A, and the numerical details outlined in Sec. II B. Section III A presents the velocity and vorticity fields of the solution. The relation of the model problem to a three-dimensional jet in cross-flow is discussed in Sec. III C, and a pressure-based argument to explain the solution is presented in Sec. IV. The paper ends with a brief summary in Sec. V.

II. MODEL PROBLEM

A. Problem statement

A two-dimensional model problem is studied in order to understand the evolution of the jet cross section. The initial condition of the problem is shown in Fig. 2. Note that only a part of the domain is shown. A circular region of diameter d is defined. The fluid inside this region has a uniform out-of-plane velocity $(v=v_j)$ and zero in-plane velocity $(u,w=0)$.

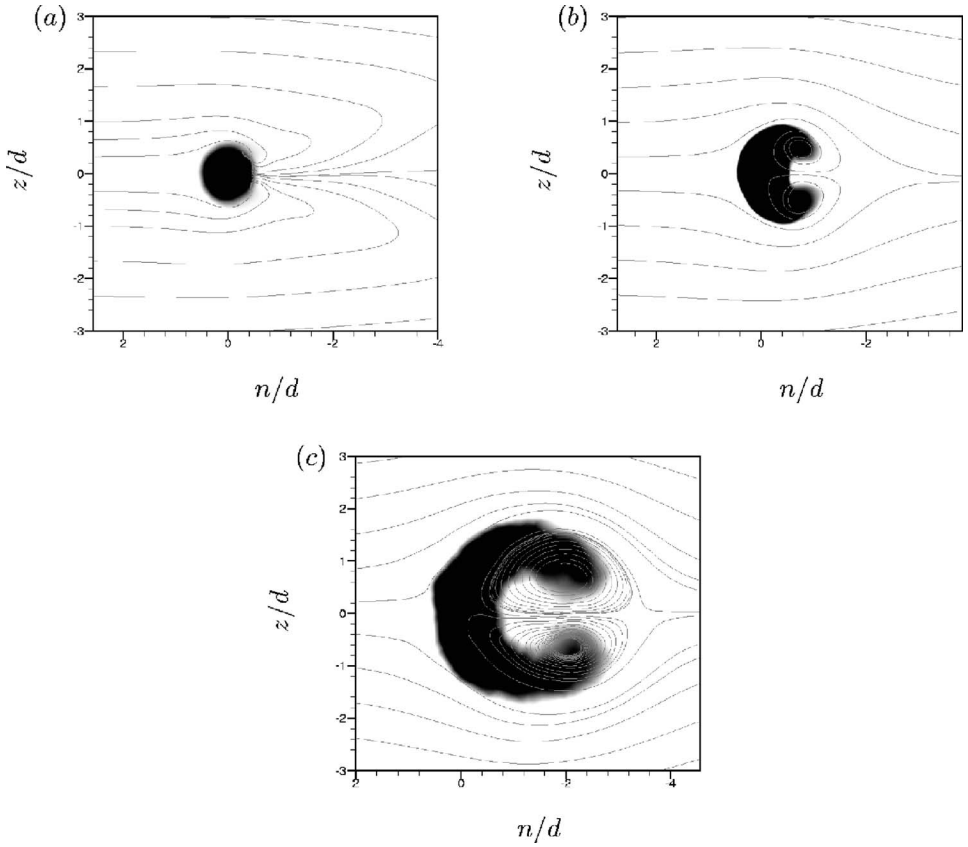

FIG. 1. Contours of time-average out-of-plane velocity shown on planes normal to the jet length. (a) $s=d$, (b) $s=3d$, and (c) $s=7d$. Note the increase in the size, and the change in shape, of the jet cross section. The direction of cross-flow fluid in these plots is from the left to the right. These results are from direct numerical simulation of a turbulent jet in cross-flow (Ref. 15), $\mathrm{Re}_{\mathrm{jet}}=5000$, $r=5.7$.

The fluid outside this region is prescribed to have an in-plane velocity (u,w) corresponding to potential flow past a circular cylinder, and a zero out-of-plane velocity $(v=0)$. The fluid inside the circle simulates the jet and the fluid outside of it simulates the cross-flow. The direction of the cross-flow fluid is from left to right. Uniform cross-flow velocity (u_∞) is specified at the inflow and the spanwise boundaries. The evolution of the jet in a three-dimensional transverse jet is spatial (moving away from the jet exit) while the evolution of the jet in the model problem is temporal.

The parameters in the model problem that can be independently controlled are the cross-flow velocity (u_∞), the jet velocity (v_j), the diameter (d), and the kinematic viscosity (ν). The velocity ratio $r=v_j/u_\infty$. To study the behavior of the model problem at different r, u_∞ was changed while keeping the jet velocity constant. The effect of Reynolds number on the solution was studied by varying ν. Simulations are performed at Reynolds numbers $(\mathrm{Re}=u_\infty d/\nu)$ of 1000, 5000, 10 000, and 100 000. Computational meshes with varying mesh sizes were used to perform preliminary simulations and to study grid convergence. The results presented in this paper are from grid converged solutions, and pertain to simulations performed on a mesh with uniform edge lengths $\Delta x/d=0.005$ and $\Delta z/d=0.005$.

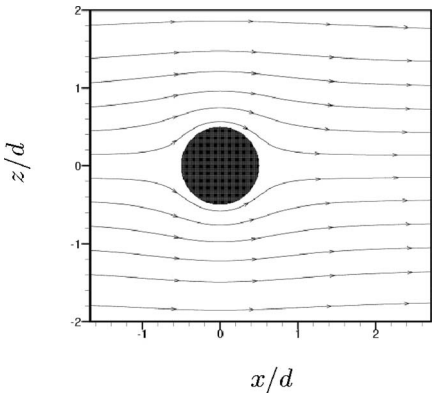

FIG. 2. Initial condition of the model problem used to study the evolution of the jet. Streamlines show the potential flow past a circular cylinder, while the contours show out–of–plane velocity.

B. Numerical details

The numerical scheme solves the incompressible Navier Stokes equations on unstructured grids. The density of the fluid is assumed constant and is absorbed into the pressure. The numerical scheme is described in Mahesh *et al.*[12] The algorithm stores the Cartesian velocities and the pressure at the centroids of the cells (control volumes) and the face-normal velocities are stored independently at the centroids of the faces. The scheme is a predictor-corrector formulation that emphasizes discrete energy conservation on unstructured grids. This property makes the algorithm robust at high Reynolds numbers without numerical dissipation. The predicted velocities at the control volume centroids are obtained using the viscous and the nonlinear terms of the momentum equation, which are then used to predict the face-normal velocities on the faces. The predicted face-normal velocity is projected so that continuity is discretely satisfied. This yields a Poisson equation for pressure that is solved iteratively using

a multigrid approach. The pressure field is used to update the Cartesian control volume velocities. Time-advancing is performed using the Adams-Bashforth scheme. The algorithm has been validated for a variety of problems (see Mahesh *et al.*[12]) over a range of Reynolds numbers.

III. SOLUTION

A. Velocity field

The model problem is effectively two-dimensional and, hence, derivatives in the y direction vanish. The governing equations for momentum reduce to

$$\frac{\partial u}{\partial t}+u\frac{\partial u}{\partial x}+w\frac{\partial u}{\partial z}=-\frac{\partial p}{\partial x}+\nu\left\{\frac{\partial^2 u}{\partial x^2}+\frac{\partial^2 u}{\partial z^2}\right\},$$

$$\frac{\partial w}{\partial t}+u\frac{\partial w}{\partial x}+w\frac{\partial w}{\partial z}=-\frac{\partial p}{\partial z}+\nu\left\{\frac{\partial^2 w}{\partial x^2}+\frac{\partial^2 w}{\partial z^2}\right\}, \text{ and} \qquad (1)$$

$$\frac{\partial v}{\partial t}+u\frac{\partial v}{\partial x}+w\frac{\partial v}{\partial z}=\nu\left\{\frac{\partial^2 v}{\partial x^2}+\frac{\partial^2 v}{\partial z^2}\right\}.$$

Note that u and w are not affected by the out-of-plane velocity component v, and that the equation governing v is the same as that governing passive scalar transport. The contours of v, hence, accurately represent the jet fluid on the x-z plane.

The jet cross section at different instants of time is shown in Fig. 3 using contours of velocity (v). These figures correspond to a simulation where $u_\infty = v_{\text{jet}} = 1.0$. Figures 3(a)–3(d) show the solution of the model problem at Re $=1000$ and Figs. 3(e)–3(h) show the solution at Re$=10\,000$. Note that figures in the same row correspond to the same time instant. Also, the oscillations observed exterior to the jet are part of the solution and do not result from the numerics. These oscillations appear to be aligned with the local curvature of the jet and are resolved on the grid. The sequence of Figs. 3(a)–3(d) shows that the initially circular jet begins to flatten at the trailing edge, resulting in a kidney-shaped cross section. The trailing edge continues to move toward the leading edge, forming a partial "ring" of jet fluid around cross-flow fluid [Fig. 3(d)]. Note that by this stage in the evolution of the jet, the edges begin to roll up indicating a concentration of vorticity and the early stages in CVP formation.

By comparing Figs. 3(d) and 3(h), it can be observed that the jet deformation is slower at the higher Reynolds number. Also, note that the jet at the higher Reynolds number has moved a smaller distance in the direction of the cross-flow. The Reynolds number also affects the presence of instabilities on the jet edge. At the lower Reynolds number, no instabilities are observed. At Re$=10\,000$, Figs. 3(e)–3(h) show "rollers" on the top and bottom edges of the jet. Since the cross-flow velocity field is initially that of potential flow past a cylinder, shear is greatest at the top and bottom edges of the jet. This results in the Kelvin-Helmholtz instability mechanism being active on these edges. The initial stages of this instability are observed in Fig. 3(f) and the ensuing "rollers" are observed in Figs. 3(g) and 3(h).

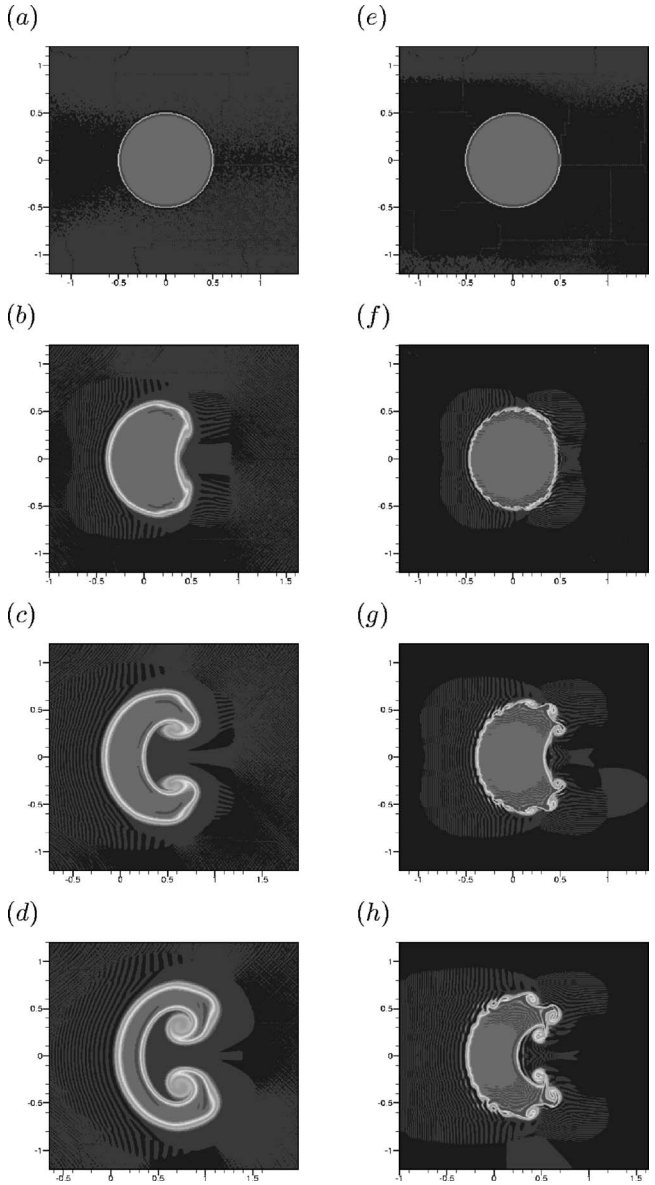

FIG. 3. Behavior of the solution of the model problem. (a)–(d) Re$=1000$, (e)–(h) Re$=10\,000$. Only part of the domain is shown.

The cross sections of the jet at a much later instant in time are shown in Fig. 4. The figures correspond to a quasi-steady-state where the jet translates in the direction of the cross-flow with a constant velocity u_{final}. The two plots are

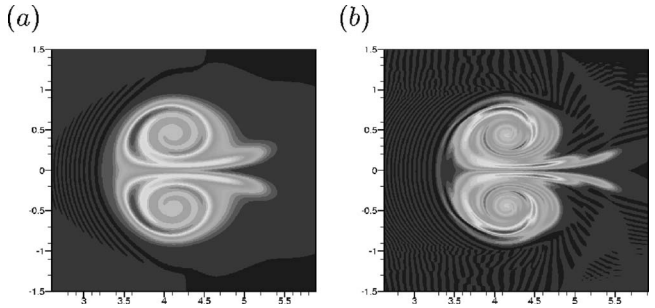

FIG. 4. Final stage in the evolution of the jet in the model problem. (a) Re$=1000$ and (b) Re$=10\,000$. The counter-rotating vortex pair is clearly seen.

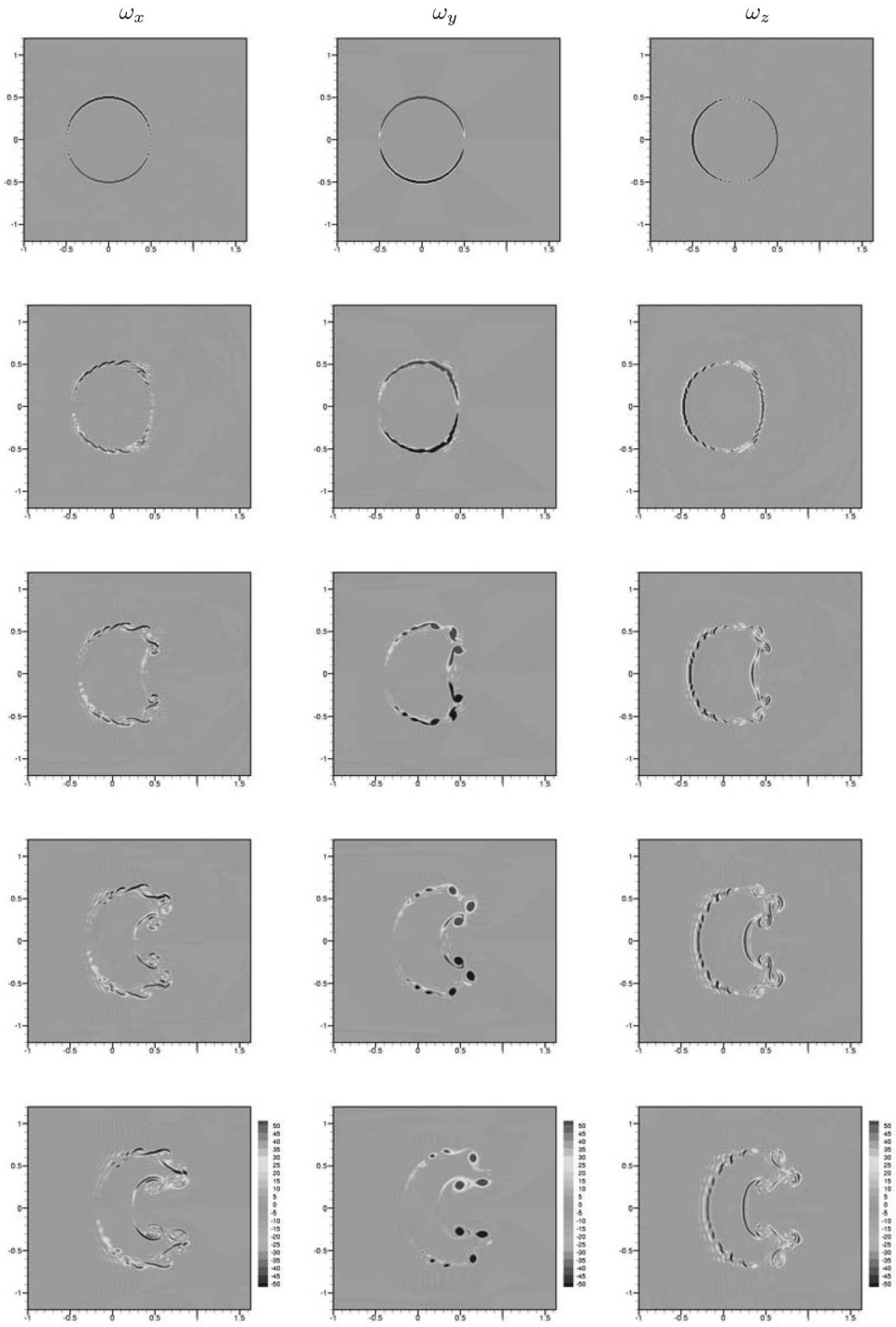

FIG. 5. Evolution of vorticity around the jet with time. The horizontal and vertical axes are x/d and z/d, respectively. Figures in each row are at the same time instant. $u_\infty = v_j$; $Re_{cf} = 10\,000$.

not at the same instant of time. The jet at Re=1000 reaches this state earlier than the jet at Re=10 000. Note that even at the higher Reynolds number, the instabilities on the jet edge are absent, and the counter-rotating vortex pair (CVP) is clearly visible. Two aspects about the jet in this regime merit mention. The separation distance between the concentrated vortices appears to be the same at both the Reynolds numbers, and the translation velocity (u_{final}) is less than the free-stream velocity u_∞. Moreover, u_{final} is a function of the Reynolds number, and an increase in the Reynolds number causes u_{final} to decrease. This aspect of the jet's evolution is discussed in detail in Sec. III B.

Under the conditions of the model problem, the vorticity components reduce to

$$\omega_x = -\frac{\partial v}{\partial z}, \quad \omega_y = \frac{\partial u}{\partial z} - \frac{\partial w}{\partial x}, \quad \text{and} \quad \omega_z = \frac{\partial v}{\partial x}. \tag{2}$$

Figure 5 shows vorticity contours in the vicinity of the jet for a simulation where Re=10 000 and $u_\infty = v_j$. Plots in each horizontal row show the solution at the same time instant. The initial condition of the problem specifies that all the vorticity is distributed along the jet circumference, as is observed in the top row of the figure. As the jet cross section

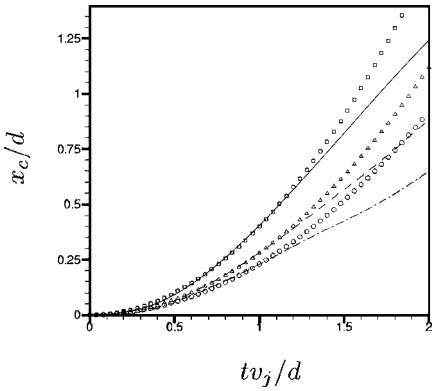

FIG. 6. Position of the jet plotted against time. ——, Re=1000; - - - -, Re=10 000; and –·–, Re=100 000. Symbols show quadratic curve fits to each of the trajectories. $u_\infty = v_j$ for all the plots.

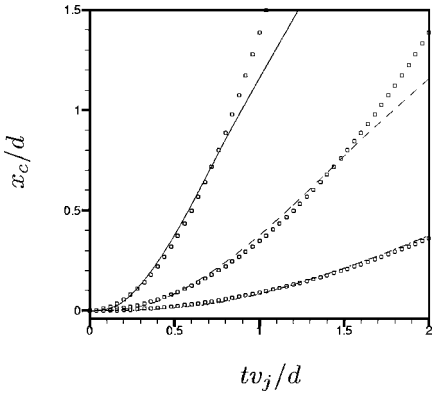

FIG. 7. Position of the jet plotted against time. ——, r=0.5; - - - -, r=1.0, and –·–, r=2.0. Symbols show quadratic curve fits to each of the trajectories. $\mathrm{Re}_{cf}=10000$ for all the cases.

evolves, vorticity contours indicate the instabilities along the jet edge. ω_y is observed to accumulate into Kelvin-Helmholtz rollers whose size increases toward the trailing edge of the jet. Further in time, the regions of concentrated ω_y merge, giving rise to the CVP as seen in Figs. 4(a) and 4(b).

B. Jet center variation with time

Figure 6 shows the evolution of the center of the jet with time. The center of the jet is defined as the centroid of the vertical velocity (v):

$$x_c = \frac{\int\int_D v x \mathrm{dA}}{\int\int_D v \mathrm{dA}},$$

where D is the complete flow domain in the x-z plane. Also shown are quadratic fits to each of the trajectories, denoted by symbols. The initial trajectory of the jet is quadratic while the latter trajectory is linear. This suggests that initially, the jet experiences a constant acceleration in the direction of the cross-flow, and that it moves at a constant velocity (u_{final}) at a later time ($tv_j/\mathrm{d} > 1.0$ for Re=1000, from Fig. 6). The acceleration of the jet (in the accelerating regime) and the velocity of the jet (in the constant-velocity regime) appear to depend on the Reynolds number. Figure 6 shows that as the Reynolds number increases, the jet experiences a lower initial acceleration, and that the later–stage velocity is also lower.

The acceleration of the jet (a_{jet}) can be explained in terms of the pressure gradient imposed on it by the cross-flow fluid and imagined to be the result of competing inertias of the cross-flow fluid (in the x direction) and the jet fluid (in the y direction), similar to the analysis of the jet trajectory presented by Muppidi and Mahesh.[13] It follows that along with the Reynolds number, a_{jet} depends on the momentum of the cross-flow fluid and that of the jet fluid. Intuitively, as the cross-flow momentum increases, the pressure gradient that the cross-flow fluid imposes on the jet increases, as does a_{jet}. As the velocity ratio increases, the jet momentum increases, causing a_{jet} to decrease. Figure 7 shows the time history of the center of the jet at different velocity ratios. Reynolds number ($\mathrm{Re}_{cf}=u_{cf}d/\nu$) for all the simulations is the same, at 10^4. The curves in Fig. 7 indeed show that an increase in the velocity ratio causes the acceleration of the jet to decrease. The symbols show quadratic curve fits to these trajectories. By evaluating the constants to these curve fits, a_{jet} can be computed. The acceleration at $r=0.5$, 1.0, 2.0, and 4.0 is 2.773, 0.693, 0.185, and 0.039, respectively, showing the dependence of a_{jet} on r to be

$$a_{\mathrm{jet}} \propto \frac{1}{r^2}. \tag{3}$$

Figure 6 shows the effect of Reynolds number (at a fixed r) and Fig. 7 shows the effect of r (at a fixed Re_{cf}) on the time history of the jet center. Clearly, the jet trajectory depends on both of these parameters. To compare their relative effects, Fig. 8 shows the jet trajectory for cases (a) $r=1.0$, $Re_{cf}=10\,000$; (b) $r=2.0$, $Re_{cf}=5000$; and (c) $r=2.0$, $Re_{cf}=10\,000$. The acceleration of the jet increases with a decrease in either Re_{cf} or r. However, the effect of changing r is more pronounced than that of changing Re by the same factor.

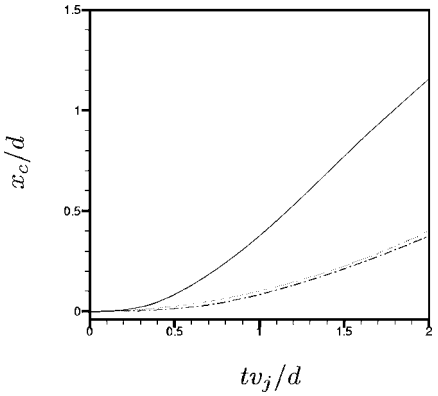

FIG. 8. Position of the jet plotted against the time. ——, r=1.0 and $\mathrm{Re}_{cf}=10\,000$; ……, r=2.0 and $\mathrm{Re}_{cf}=5000$; –·–, r=2.0 and $\mathrm{Re}_{cf}=10\,000$.

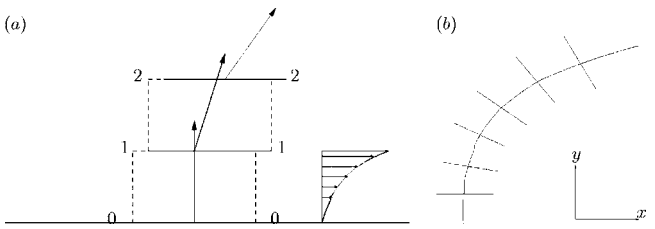

FIG. 9. (a) Galilean transformation of the model jet as it evolves in time. (b) Trajectory of the jet.

C. Relation to 3D jets in cross-flow

The model problem is qualitatively related to a three-dimensional (3D) transverse jet as follows. Close to the jet exit, the jet fluid has no velocity in the direction of the cross-flow. The cross-flow fluid accelerates the jet fluid in its direction, causing the jet to bend. Consider the schematic in Fig. 9(a). At the initial condition (given by 0-0), the jet has a velocity v_j in the y direction, $u_j=0$, and the vorticity vector (of magnitude ω_y) also points in the y direction. Consider the jet after an interval dt shown by 1-1. Due to the acceleration imposed by the cross-flow fluid, the jet gains a velocity u_j in the x direction. In the absence of u_j, the jet cross section would be displaced only in the y direction (as shown by the dashed lines). A nonzero u_j, however, displaces the jet both in x and y directions (shown by the solid lines). Note that as a result of the acceleration of the jet, the jet velocity vector changes direction between 0-0 and 1-1. With increasing time, the displacement of the jet yields the trajectory, shown in Fig. 9(b).

In a three-dimensional jet, bending of the jet is also associated with tilting of the vorticity. Consider the evolution of vorticity vector (of the jet in the model problem) between time $t=0$ and $t=dt$. At $t=0$, $\omega_x=\omega_z=0$. ω_y, however, is nonzero. $v=v_j$ and $u_j=0$. Past the initial condition, the jet accelerates in the x direction. That is, $\partial u/\partial t \neq 0$. By a Galilean transformation, this $\partial u/\partial t$ corresponds to $\partial u/\partial y$ for a three-dimensional transverse jet. Consider the equation for the evolution of vorticity

$$\frac{\partial \omega_i}{\partial t} + \text{convection} = \omega_j \frac{\partial u_i}{\partial x_j} + \text{dissipation},$$

where $\omega_j(\partial u_i/\partial x_j)$ is the *stretching/tilting* term. Between $t=0$ and dt, a nonzero ω_y and a nonzero $\partial u/\partial y$ result in the production of the x direction component of the vorticity, ω_x. The displacement of the jet and the deformation of the jet cross section are accompanied, therefore, by a tilting of the vorticity vector.

Initially, the jet and cross-flow directions are perpendicular to each other, and the relevance of the model problem to the three-dimensional transverse jet is clear. The model problem does not directly account for the bending of the jet, and past the near-field, the relationship with the transverse jet is qualitative. Consider the schematic of the jet shown in Fig. 10. At a station where the jet is no longer vertical, consider the plane normal to the jet trajectory (shown by the dashed lines). $u_{crossflow}$ is the free-stream cross-flow velocity, and u_∞ is the cross-flow velocity in the model problem. The acceleration (a_{jet}) and velocity (u_j) of the jet, predicted by the model problem, describe the evolution of the jet cross section (in a three-dimensional transverse jet) in the trajectory normal plane. In a transverse jet, the in-plane cross-flow velocity (u_∞) decreases with decreasing angle between the jet and the cross-flow. Also, v_j decreases along the jet length. In the two-dimensional model problem, u_∞ is a constant.

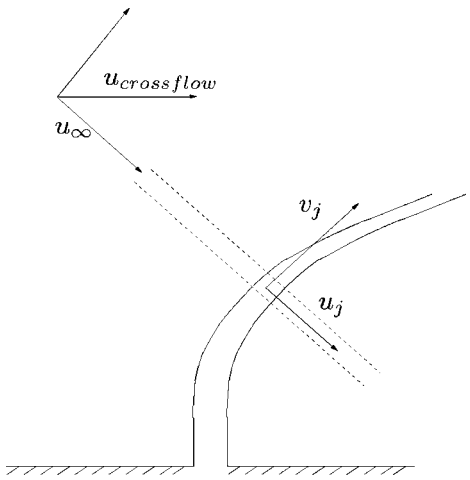

FIG. 10. Schematic showing the relevance of the model jet problem as the three-dimensional jet begins to bend.

Qualitatively, the figures showing the evolution of the jet cross section in the three-dimensional jet in cross-flow (Fig. 1) are similar to those showing the evolution of the jet in the model problem (Fig. 3). The cross sections in both cases are almost circular in the beginning [Figs. 1(a) and 3(a)]. The deformation in both cases begins with a flattening of the trailing edge. Figures 1(b) and 3(b) both show the trailing edge to move toward the leading edge and the jet to acquire a "kidney-shaped" cross section. The thickness of the jet on the symmetry line continues to decrease in both the cases [1(c) and 3(c)], and the jets exhibit a shape in which the high velocity (out-of-plane component) fluid surrounds the low-velocity cross-flow fluid.

Formation of the CVP and the deformation of the jet are simultaneous phenomena. They occur at a rate determined by a_{jet} which, in turn, depends on both the Reynolds number and the cross-flow momentum (and, hence, r). Consider two jets at velocity ratios 10 and 20. Recalling that $a_{\text{jet}} \propto 1/r^2$, a_{jet} for the $r=20$ jet decreases to a quarter of a_{jet} at $r=10$. If it is assumed that the rate of evolution of the jet is proportional to the acceleration, it follows that the two jets will not exhibit

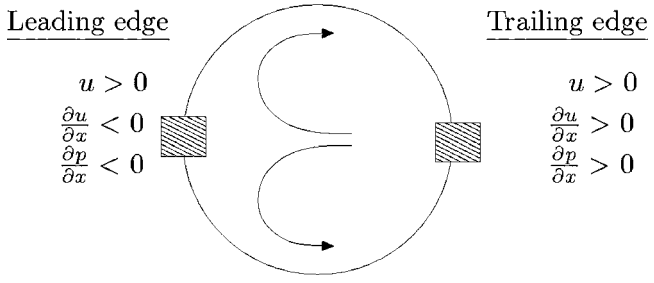

FIG. 11. Schematic of the jet cross section.

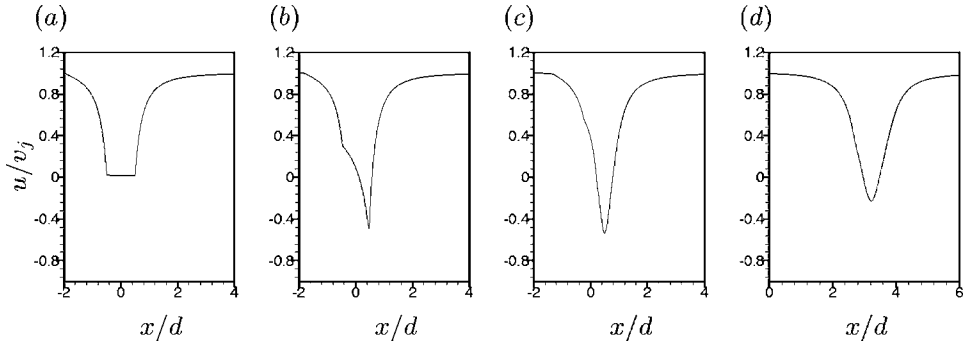

FIG. 12. Profiles of velocity u along the symmetry line at increasing instants of time.

similar CVP development (and jet deformation) at the same point in an rd–coordinate system, but rather in an r^2d-coordinate system. In other words, CVP development of the $r=20$ jet occurs farther downstream in the rd space as compared to the $r=10$ jet, a fact that was reported by Smith and Mungal[6] (Fig. 9). It must be mentioned that the results shown in that work correspond to the same Re_{jet}. The Reynolds number based on the cross-flow, therefore, is different by a factor of 2, and the observed difference in the rate of CVP formation is a consequence of a change in r *and* a change in Re_{cf}. However, Fig. 8 shows that the effect of doubling Re_{cf} on the jet acceleration is negligible, compared to that of doubling r. Note that the velocity ratio r affects the far-field behavior in two ways: (i) the near-field acceleration and (ii) the local velocity ratio (v_j/u_∞) along the jet length. The 2D model accounts for (i) but not (ii). Our inferences regarding the far field are therefore qualitative.

The concentration of the vorticity and the formation of the CVP in the model problem seem to suggest that the pipe is not necessary for the formation of the CVP in transverse jets as suggested by some past studies (e.g., Ref. 9). The pressure and velocity field in the vicinity of the jet cause the CVP to be formed slightly downstream of it, and it appears that the contribution to vorticity of the CVP comes from the vorticity in the jet shear layer. Kelso *et al.*[5] suggest that there is a connection between the CVP roll-up and the separation inside the pipe. In view of the present results, it appears that while the separation might contribute to the formation of the CVP, it does not cause the formation. In addition, separation (and the resulting separation streamlines on the pipe surface) inside the pipe is not evident as jet-to-cross-flow velocity ratio increases.

Interestingly, aspects of the solution to the model problem bear similarities to the behavior of a drop subject to a high-speed airstream. Joseph *et al.*[14] report that such a drop exhibits a constant acceleration in the initial stages. A change in shape is also observed. The drop, which is initially spherical, begins to acquire a flattened trailing edge and the trailing edge continues to move toward the leading edge (prior to the drop breakup), just as in the solution to the model problem.

IV. EXPLANATION

The evolution of the jet can be summarized as follows. Cross-flow fluid pushes the jet fluid in its direction. While the jet accelerates (to the right, in the context of the present problem), the trailing edge moves toward the leading edge. The jet expands radially, and the cross section deforms. The shear is maximum on the top and bottom edges, and the Kelvin-Helmholtz instability is observed. The flow field and the deformation cause the vorticity in the shear layer to redistribute, and ω_y concentrates toward the downstream side of the jet. The jet moves with a constant acceleration, initially, and with a constant velocity at later stages. This section attempts to explain these phenomena.

Initially, the jet fluid has no streamwise velocity. The streamwise momentum of the cross-flow, therefore, accelerates the jet in the direction of the cross-flow. Recall that the x-direction equation for momentum is

$$\underset{1}{\frac{\partial u}{\partial t}} + \underset{2}{u\frac{\partial u}{\partial x}} + \underset{3}{w\frac{\partial u}{\partial z}} = \underset{4}{-\frac{\partial p}{\partial x}} + \underset{5}{\nu\left\{\frac{\partial^2 u}{\partial x^2} + \frac{\partial^2 u}{\partial z^2}\right\}}. \tag{4}$$

Consider a control volume that contains the leading edge of the jet, at an instant close to the initial condition, as shown in Fig. 11. By symmetry, w and, hence, term 3 are zero. Figure 12 shows the streamwise profiles of velocity u on the symmetry line at different instants of time. These profiles are

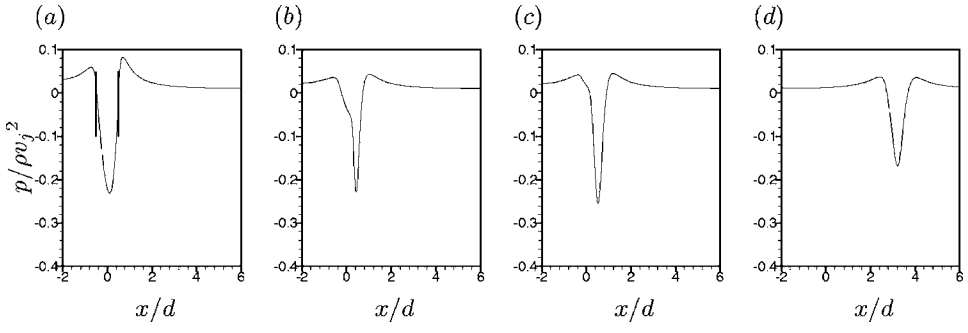

FIG. 13. Profiles of pressure along the symmetry line at increasing instants of time. The vertical lines in (a) indicate the edges of the jet.

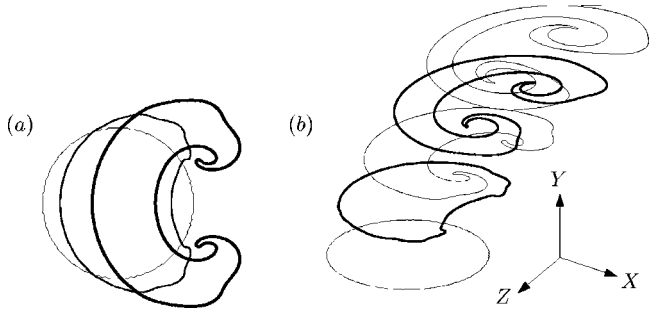

FIG. 14. Schematic to show the stages of evolution of the jet cross section. The two-dimensional cross sections are arranged along the y direction in (b).

from a simulation where $u_\infty = v_j$. Figures 12(a)–12(c) plot the velocity profile at time instants soon after the initial condition and Fig. 12(d) plots the profile at a later time instant. According to the initial condition, the jet fluid has no streamwise velocity, as shown in Fig. 12(a). Along the x axis, the velocity of the cross-flow fluid decreases moving closer to the leading edge. The slope of this variation (down from u_∞ to zero) depends on the viscosity. Past the jet's trailing edge, u increases. At later instants, a negative velocity is observed within the jet indicating a reverse flow. As the jet evolves, the peak negative velocity decreases in magnitude. At the leading edge of the jet, as can be observed from Fig. 12,

$$u > 0 \quad \text{and} \quad \frac{\partial u}{\partial x} < 0,$$

making the second term in Eq. (4) negative.

From the initial condition, it follows that the maximum pressure occurs near the leading and trailing edges of the jet. Figure 13 shows the streamwise variation of pressure at different instants of time. The edges of the jet are indicated in Fig. 13(a). Note that the pressure increases along the x axis and reaches a peak just upstream of the jet edge. Past this point, the pressure decreases and the pressure minima are observed within the jet. Downstream of the jet's trailing edge, another pressure peak is observed. The first three plots show profiles at time instants soon after the initial condition, and the last profile plots the pressure at a much later instant in time. From Fig. 13(a), it is easy to see that at the leading edge, $\partial p/\partial x < 0$. For the purpose of the present analysis, and considering that the range of ν for the set of simulations presented here is $[10^{-4}, 10^{-6}]$, term 5 can be neglected.

Hence, for the control volume at the leading edge,

$$\frac{\partial u}{\partial t} = -\frac{\partial p}{\partial x} - u\frac{\partial u}{\partial x} > 0.$$

In contrast, at the trailing edge,

$$u > 0, \quad \frac{\partial u}{\partial x} > 0 \quad \text{and} \quad \frac{\partial p}{\partial x} > 0.$$

A similar analysis for a control volume containing the trailing edge of the jet shows that $\frac{\partial u}{\partial t} < 0$. Therefore, the leading edge of the jet accelerates in the direction of the cross-flow, while the trailing edge decelerates. The increase in u at the leading edge and the decrease in u at the trailing edge are clearly observed by contrasting Figs. 12(a) and 12(b). Jet fluid in the vicinity of the trailing edge is pushed toward the leading edge (causing a reverse flow and a negative u velocity). In order to satisfy continuity, some of the jet fluid is forced radially outward from the symmetry plane. The jet boundary acts as a limiting streamline, and symmetric recirculation regions are set up within the jet, as indicated by the streamlines in Fig. 11. The jet cross section is compressed in the horizontal direction causing the jet to expand in the vertical (z) direction, leading the cross section to evolve as shown in Fig. 14(a). As the jet cross section deforms, concentration of ω_y causes a roll up, and the formation of a CVP. An interesting way to look at the jet deformation is to stack the jet cross sections in space, along the third dimension (y). Such a perspective is shown in Fig. 14(b). Successive plots are displaced in y by the same distance.

In the constant velocity regime (Fig. 4), the local flow field appears dominated by the CVP. Figure 15 shows the variation of ω_y, u, and p along the spanwise variable z in this regime. $u_\infty = v_j$ and $\mathrm{Re}_{cf} = 1000$. These profiles are plotted at $x \sim 5d$, and along a line passing through the center of the CVP. Vorticity profile [Fig. 15(a)] clearly shows the presence of two concentrated, counter-rotating vortex regions. The vorticity is negligible past a distance d from the symmetry line and the centers of the vortices are indicated by peak ω_y. Figure 15(b) shows that away from the symmetry line ($z = 0$), streamwise velocity (u) is u_∞. Moving closer to the jet, the velocity peaks near the edge of the jet. Moving further toward the symmetry line, u decreases. Figure 15(c) plots the pressure. Away from the symmetry line, the pressure corre-

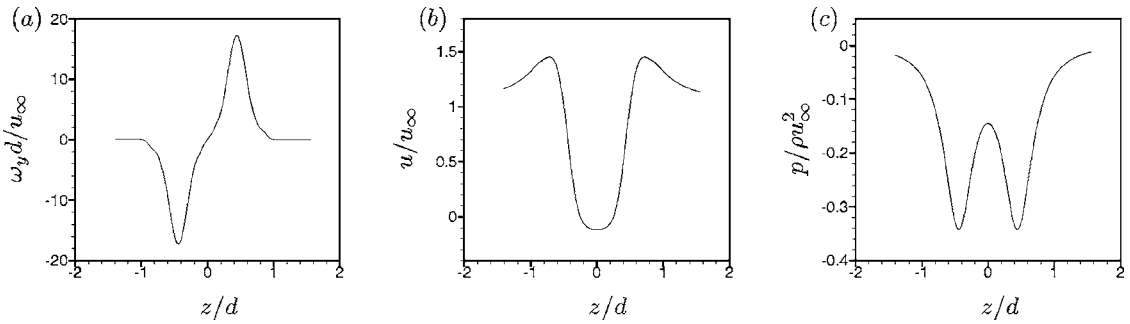

FIG. 15. Profiles of out-of-plane vorticity ω_y, velocity u, and pressure plotted against the spanwise distance variable. Re=1000, $u_\infty = v_j = 1.0$.

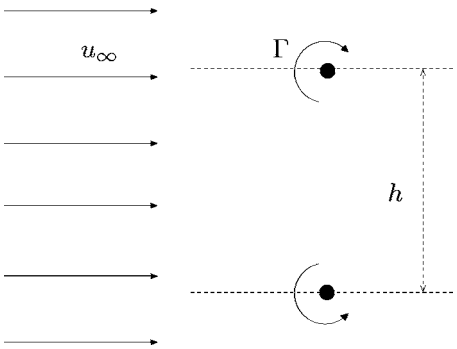

FIG. 16. Schematic of the flow in the far field, dominated by the counter-rotating vortex pair.

sponds to a free-stream pressure. Moving closer to the symmetry line, the pressure decreases. The minimum pressure corresponds to the center of the vortices.

The jet in this stage can be visualized as a pair of counter-rotating vortices translating in the direction of the cross-flow fluid, as shown by the schematic in Fig. 16. Note that Fig. 16 bears similarity to the classical representation of the far field of a transverse jet (e.g., Fig. 4 in Ref. 11). Let Γ be the circulation of each of the vortices and h be the separation distance between them. Each vortex induces a velocity $u_{\text{induced}}=\Gamma/2\pi h$ on the other. Note that the direction of this induced velocity is opposite to that of the cross-flow velocity. The cross-flow fluid attempts to accelerate the jet and to increase u_{jet}. In the absence of the CVP, u_{jet} would be expected to increase to u_∞ and remain constant. The induced velocity due to the vortex pair attempts to decelerate the jet. An equilibrium stage can be imagined, where the velocities satisfy

$$u_\infty - u_{\text{induced}} = u_{\text{final}}.$$

The jet continues to accelerate until u_{jet} reaches u_{final} and the jet translates at this constant velocity thereafter. The dependence of u_{final} on the Reynolds number is presented in Table I.

It is seen that the effect of increasing the Reynolds number is to increase u_{induced} and to decrease u_{final}. This can be explained as follows. At a constant cross-flow velocity, u_{final} depends on u_{induced}, which depends on Γ. The total circulation in the domain, stipulated by the initial condition, is a function only of the relative velocity of the (cross-flow) fluid past the jet fluid. Past the initial condition, viscosity dictates the circulation decay. As the Reynolds number decreases, the decay in circulation is higher, resulting in a lower Γ. Hence, a smaller value of u_{induced} and a higher value of u_{final} are obtained.

TABLE I. Variation of translation velocity (u_{final}) in the constant-velocity regime with Reynolds number.

v_j/u_∞	Re	$u_{\text{final}}/u_\infty$	$u_{\text{induced}}/u_\infty$
1	1000	0.784	0.2160
1	10000	0.684	0.3160
1	100000	0.488	0.5120

V. SUMMARY

A two-dimensional model problem is used to study the evolution of a jet in cross-flow. Using the solution to the model problem, the deformation of the jet cross section can be explained in terms of the pressure field around the jet, and the initial acceleration that the jet fluid experiences in the direction of the cross-flow. The solution to the model problem also yields the CVP, indicating that the pipe is not necessary for the formation of the CVP. The evolution of the jet is a function of both the velocity ratio and the Reynolds number. The dependence of the jet acceleration on the cross-flow velocity explains the experimentally observed dependence of the CVP formation on the velocity ratio.

ACKNOWLEDGMENTS

This work was supported by the National Science Foundation under Grant No. CTS–0133837. Computer time was provided by the National Center for Supercomputing Applications (NCSA), Minnesota Supercomputing Institute (MSI), and the San Diego Supercomputer Center (SDSC). We thank Professor D. Joseph and Professor T. Lundgren for useful discussions.

[1] Y. Kamotani and I. Greber, "Experiments on turbulent jet in a crossflow," AIAA J. **10**, 1425 (1972).
[2] R. L. Fearn and R. P. Weston, "Vorticity associated with a jet in cross-flow," AIAA J. **12**, 1666 (1974).
[3] J. F. Keffer and W. D. Baines, "The round turbulent jet in a cross wind," J. Fluid Mech. **15**, 481 (1963).
[4] B. D. Pratte and W. D. Baines, "Profiles of the round turbulent jet in a cross flow," J. Hydr. Div. **92**, 53 (1967).
[5] R. M. Kelso, T. T. Lim, and A. E. Perry, "An experimental study of round jets in cross-flow," J. Fluid Mech. **306**, 111 (1996).
[6] S. H. Smith and M. G. Mungal, "Mixing structure and scaling of the jet in crossflow," J. Fluid Mech. **357**, 83 (1998).
[7] J. E. Broadwell and R. E. Breidenthal, "Structure and mixing of a transverse jet in incompressible flow," J. Fluid Mech. **148**, 405 (1984).
[8] J. Andreopoulos and W. Rodi, "Experimental investigation of jets in a crossflow," J. Fluid Mech. **138**, 93 (1984).
[9] S. L. V. Coelho and J. C. R. Hunt, "The dynamics of the near field of strong jets in crossflows," J. Fluid Mech. **200**, 95 (1989).
[10] L. Cortelezzi and A. R. Karagozian, "On the formation of the counter-rotating vortex pair in transverse jets," J. Fluid Mech. **446**, 347 (2001).
[11] A. R. Karagozian, "An analytical model for the vorticity associated with a transverse jet," AIAA J. **24**, 429 (1986).
[12] K. Mahesh, G. Constantinescu, and P. Moin, "A numerical method for large-eddy simulation in complex geometries," J. Comput. Phys. **197**, 215 (2004).
[13] S. Muppidi and K. Mahesh, "Study of trajectories of jets in crossflow using direct numerical simulations," J. Fluid Mech. **530**, 81 (2005).
[14] D. D. Joseph, G. S. Beavers, and T. Funada, "Rayleigh–Taylor instability of viscoelastic drops at high Weber numbers," J. Fluid Mech. **453**, 109 (2002).
[15] S. Muppidi and K. Mahesh, "Direct numerical simulation of turbulent jets in crossflow," AIAA Pap. 2005-1115 (2005).